Development of Ti02/RT-35HC based nanocomposite phase change materials (NCPCMs) for thermal management applications.

Adeel Arshad", Mark Jabbala, Lei Shia'b , Jo Darkwac, Nicola J. Westond, Yuying Yana,"

'Fluids & Thermal Engineering (FLUTE) Research Group, Faculty of Engineering, University of Nottingham, Nottingham NG7 2RD, UK

b School of Energy Science and Engineering, Harbin Institute of Technology, Harbin 150001, China

Building, Energy and Environment (BEE) Research Group, Faculty of Engineering, University of Nottingham, Nottingham NG7 2RD, UK

dNanoscale and Microscale Research Centre (nmRC), University of Nottingham, Nottingham, NG7 2RD, UK

'Research Centre for Fluids and Thermal Engineering, University of Nottingham Ningbo China, Ningbo 315100, China

Abstract

This experimental study covers the development of novel nanocomposite phase change materials (NCPCMs) based on RT-35HC as a phase change material (PCM) and titanium oxide (Ti02) as thermal conductivity enhancement material, for thermal management applications. The TiO2 loadings were varied from 0.0 to 2.0 wt.% in pure RT-35HC samples and characterized for their chemical, physical and thermal properties by different characterization methods. The microstructures, chemical structures, lattice structures showed the presence of TiO2 nanoparticles onto the surface of NCPCMs. The results revealed that thermal properties including phase—change temperature, melting/solidifying latent—heat enthalpies, specific heat capacity and thermal conductivity were decreased by the introduction of TiO2 nanoparticles. This study confirmed that NCPCMs based on Ti02/RT-35HC revealed the phase—change enthalpies and thermal conductivities of 238.33 — 227.74 J/g and 0.238 — 0.341 W/m.K, respectively. In addition, significant chemical and thermal stability and no phase segregation were observed with the increase in loading of TiO2 nanoparticles. The newly developed Ti02/RT-35HC base NCPCMs revealed acceptable chemical stability, thermal reliability, and efficient conjugate heat transfer performance. Thereby, NCPCMs exhibit the potential application for thermal energy storage and thermal management of electronic devices, Li-ion batteries and photovoltaic (PV) modules.

Keywords: Phase change material, Ti02, RT-35HC, Nanocomposite phase change

*Correspondence authors

Email addresses: adeel.arshad@nottingham.ac.uk, adeel_kirmani@hotmail. com (Adeel Arshad), yuying .yan@nottingham.ac.uk (Yuying Yan)

materials, Thermal management

1. Introduction

The recent global energy demand and supply has raised the attention of research in order to introduce efficient alternatives of thermal management (TM) and thermal energy storage (TES) systems. Specifically, the nature's blessed resources of fuels, formed by the natural processes called fossil fuels, are still being considered as key energy supply resources. However, the greenhouse emissions related to their use are still a challenge to mitigate the global climate change. The integrated systems with dual capability of TM and TES have been widely used for improving the energy efficiency and heat storage capability because of using phase change materials (PCMs) [1]. Thus, PCMs, as TES materials, have the tendency to absorb heat energy in two phase transformations (i.e. solid—to—liquid and liquid-to—solid) n and have been used air conditioning systems, desalination, refrigeration, cooling of electronic devices and electric vehicle batteries [2, 3, 4, 5]. The organic PCMs specially paraffins have been under utilization of TM and lower temperature TES systems due to their intrinsic properties of (i) higher latent—heat of fusion, (ii) durable chemical stability, (iii) desirable phase—transition temperature, (iv) lower subcooling and (v) less expenses [6]. In spite of these, paraffins also exhibt the lower thermal conductivity causing to reduce the overall heat flow rate during phase transformation [7]. Scientists and researchers have adopted a few techniques including: (i) extruded metal fins [8, 9, 10, 11], (ii) metal foams and porous materials [12, 13, 14], (iii) dispersing nanoparticles and nanofiber [15, 16, 17, 18] (iv) encapsulated micro/nano-capsules [19, 20, 21, 22] to overwhelm the thermal conductivity of PCMs.

In recent years, nanoparticles (NPs) have attracted the attention of scientists and industrialists due to their outstanding properties promoting innovation in the field of engineering and industrial processes. NPs specially the metallic—oxides have two major advantages which include: (i) structural changes which alter the lattice symmetry and cell parameters and (ii) surface properties changes which influence the thermal conductivity and chemical properties because of increase in band gap [23]. Various studies have been reported using different PCMs and NPs based on the operating conditions and melting temperature of PCMs. It is however important to consider thermal and rheological properties while endothermic/exothermic process for the determination of thermal characteristics of PCMs integrated with metallic—oxide NPs [24].

For instance Bashar and Siddiqui [25] prepared NCPCMs by dispersing MWCNT, Ag, CuO and A1203 NPs into the paraffin wax. In comparison with pure paraffin wax, the en-

34 hancement in heat transfer coefficient was achieved of 18% and 14% with CuO and Ag

35 NPs, respectively. Li et al. [26] used the 7—A1203 NPs and calcium chloride hexahydrate

36 (CaC12.6H20) as a PCM and studied the various thermal properties such as thermal con-
37 ductivity, degree of subcooling and latent—heat of melting/solidifying of composite PCMs.
38 Results reported the highest thermal conductivity of 1.373 W/m.K at 2.0 wt.% of -y—A1203
39 NPs. Sharma et al. [27] synthesized the NCPCMs using TiO2 NPs by changing the mass
40 loading of 0.5, 1.0, 3.0, and 5.0 wt.% into the palmitic acid, used as a PCM. Authors re-
41 ported the highest thermal conductivity and lowest latent—heat of 0.35 W/m.K and 180.03
42 kJ/kg 5.0 wt.% of TiO2. Sami and Etesami [28] prepared Ti02/paraffin NCPCMs with
43 weight concentration of 0.5, 0.7, 1, 2, 3 and 4 wt.% with and without sodium stearoyl lacty-
44 late (SSL) as a surfactant. Authors found the optimum concentration of TiO2 of 3 wt.%
45 resulted in 47.8% enhancement in thermal conductivity as compared to the pure paraffin. In
46 addition, they suggested that by adding the SSL as a surfactant in NCPCMs showed the
47 better dispersion and thermal stability for compared to NCPCMs without SSL.More
48 further, they suggested that NCPCMs using SLL had the better dispersion and stability of
49 TiO2 NPs compared with the with SSL NCPCMs.
50 Teng and Yu [29] prepared samples of NCPCMs with paraffin wax and by considering 1,
51 2 and 3 wt.% weight concentrations of different NPs (ZnO, Si02, TiO2 and A1203). The
52 authors found that NCPCMs containing TiO2 NPs showed better results of thermal storage
53 properties and reduced the onset decomposition temperature to make PCMs applicable to
54 heat storage and thermal management systems compared to A1203, SiO2, and ZnO nanopar-
55 titles. Wang et al. [30] prepared Ti02/paraffin wax NCPCMs with weight concentration
56 ranging from 0 — 7.0wt.% without any surfactant. They reported that the thermal conduc-
57 tivity of NCPCMs was improve till 3.0 wt.% of TiO2 and then it was decreased. Motahar
58 et al. [31] investigated the rheological and thermal properties composite PCMs of consisted
59 of n-Octadecane and TiO2 NPs with weight concentration range of 0 — 5.0 wt.%. It was
60 reported that the heat transfer occurred through conduction in solid phase and later on
61 by convection mode. However, the natural convection mode lowered the melting rate as
62 the weight concentration of TiO2 was increased because of the increase in viscosity. Chen
63 et al. [32] reported the NCPCMs synthesized by carbon—coated aluminium NPs (Al—C)

64 with paraffin wax. Authors found the thermal conductivity of 0.189 W/m.K with 4 wt.%
65 of Al—C which was 206.5% higher in comparison with paraffin wax at 25°C. Nourani et al.
66 [33, 34] prepared the paraffin wax and A1203 based NCPCMs with loading content of 0.5,

5, 7.5, and 10 wt.% of A1203 and SSL as a surfactant for better stability dispersion. For solid and liquid phases, the effective thermal conductivity enhancement was found of 31% and 13%, respectively, at **10.0** wt.%. Babapoor and his co—authors [35, 36] prepared mono and hybrid NCPCMs using SiO2, A1203, Fe2O3, ZnO NPs and investigated the thermal and phase—change properties in solid and liquid phases. Authors obtained the higher thermal diffusivity with Fe2O3 at 8 wt.%. Moreover, it was recommended that A1203 NPs were the most suitable for TM applications. Pahamli et al. [37] synthesized the NCPCMs using CuO and RT-50 by using 2 and 4 wt.%. The higher thermal conductivity enhancement was obtained of 3.9% and 7.2% with 2 wt.% and 4 wt.%, respectively. Recently, Praveen and Suresh [38] investigated the thermophysical and heat transfer characteristics using CuO and neopentyl glycol (NPG) composite PCMs. Authors found the thermal conductivity and latent—heat of 0.61 W/m.K and 112.4 kJ/kg, respectively, with 3.0 wt.% of CuO.

For effective heat storage and transfer using PCMs, the latent-heat and thermal conductivity are the key thermal properties of PCMs which improve the TM efficiency. Therefore, a PCM with higher latent—heat and thermal conductivity with stable chemical structure is the most suitable. The literature reveals that most of the studies focused on the development of NCPCMs used for the high temperature TES applications. The current study focuses on synthesising of new NCPCMs which will be the most suitable for thermal management of electronic devices, photovoltaic modules and Li-ion batteries, working under the safe and reliable operating temperature range of 30 — 40°C [39, 40]. In order to keep in mind the safe operating temperature, a commercially available PCM (RT-35HC) is selected having melting temperature of 34 — 36°C. To enhance the thermal properties and heat storage capacity at an optimum level, various loading from 0.0 to 2.0 wt.% of TiO2 nanoparticles are dispersed. In this work, various properties of NCPCMs are investigated including morphology, chemical structure, crystal phase, specific heat, thermal conductivity, phase—change thermal properties, thermal stability and reliability.

2. Experimental description

2.1. Materials

In this work, the RT-35HC (34 — 36°C) was selected as a PCM which is commercially available product by Rubitherm GmbH, Germany, categorized under the paraffin PCMs. Nano Titanium (IV) dioxide (TiO2) [41], anatase powder (particle size < 25 nm, 99.7% trace metals basis, surface area: 45 — 55 m2/g, density: 3.9 g/mL at 25°C) and sodium

dodecylbenzene sulfonate (SDBS) [42] were purchased from Sigma-Aldrich, Inc. UK. The thermal properties of RT-35HC are listed in Table 1. All the materials were used without any further chemical processing because they are analytical reagent grade.

Table 1: *Thermophysical properties of RT-35HC.*

Melting temperature (°C)	Thermal conductivity (W/m.K)	Latent heat (J/kg.K)	Specific heat (J/kg.K)	Density (kg/m3)
34-36	0.2	240,000	2000	880 (solid) 770 (liquid)

2.2. Preparation of nanocomposite PCMs

For the preparation of NCPCMs, a highly precise two-step method was opted which have been used extensively to prepare the nanofluids [43], as shown in Figure 1. RT-35HC was used as a base PCM and TiO2 NPs were added with weight concentration of 0.5, 1.0, 1.5 and 2.0wt.% which acted as thermal conductivity enhancers (TCEs). In addition sodium dodecylbenzene sulfonate (SDBS) was added with the ratio 4 : 1 for each loading of the TiO2. In first step, the RT-35HC was melted completely at its liquid state by providing the heat through a hot-water bath operating at constant temperature of 70°C. To achieve the uniform dispersion of TiO2 in RT-35HC, a constant fraction of the capping agent (SDBS) was added into the liquid RT-35HC. The mixture was stirred through a magnetic stirrer homogeneously at 70°C and 450 rpm for 30 mins. Thenceforth, the TiO2 nanoparticles were added and stirred for further 3hrs for stable and uniform dispersions of TiO2 in RT-3511C. The prepared NCPCMs were labelled NCPCM1, NCPCM2, NCPCM3 and NCPCM4 for weight concentration of 0.5, 1.0, 1.5 and 2.0 wt.%, respectively. Secondly, the ultrasonication was performed of each sample of NCPCMs for 60 mins maintaining the constant temperature of 70°C using an ultrasonic vibrator at a frequency of 40kHz [44, 45]. The ultrasonication process improves homogeneous and stable dispersion of TiO2 and minimizes the agglomeration and sedimentation, as shown in Figure 2.

3. Characterization methods

The characterization of NCPCMs was carried out by various methods to study the surface morphology, chemical and physical interaction, thermal properties including phase-change temperature, melting/solidifying latent-heat enthalpies, specific heat capacity, thermal conductivity, thermal stability and thermographic images of temperature distribution.

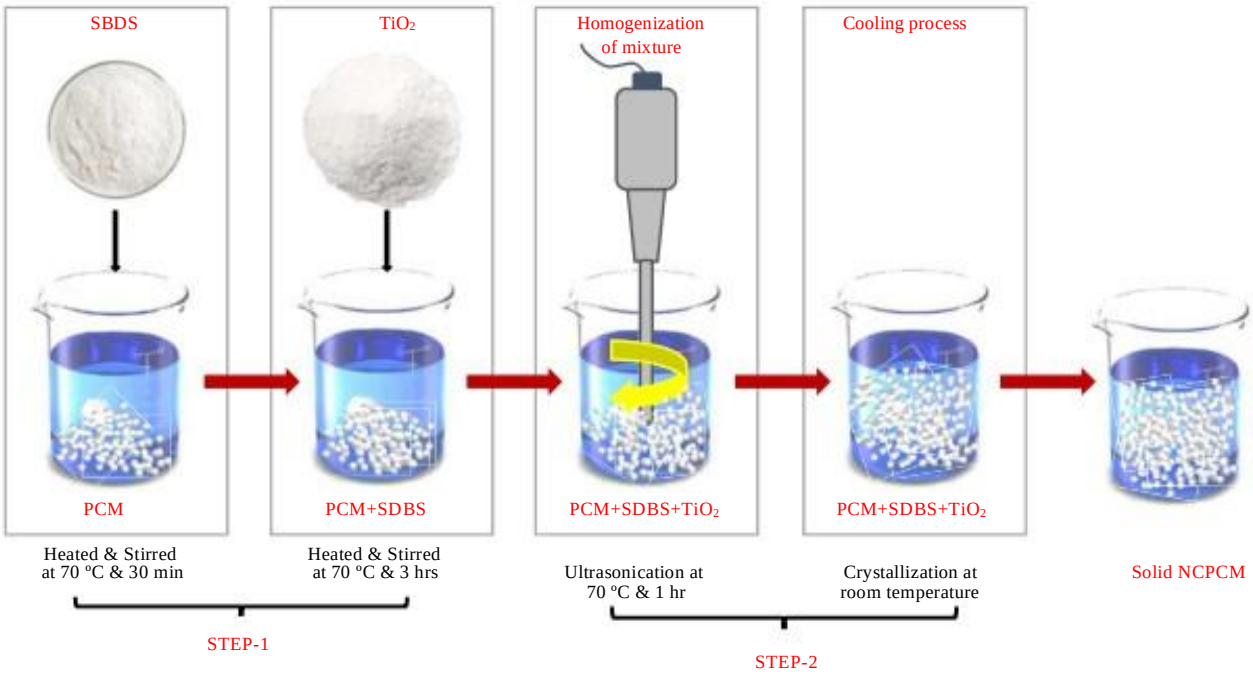

Figure 1: *Schematic diagram of sample preparation of TiO_2 and RT–35HC based NCPCMs.*

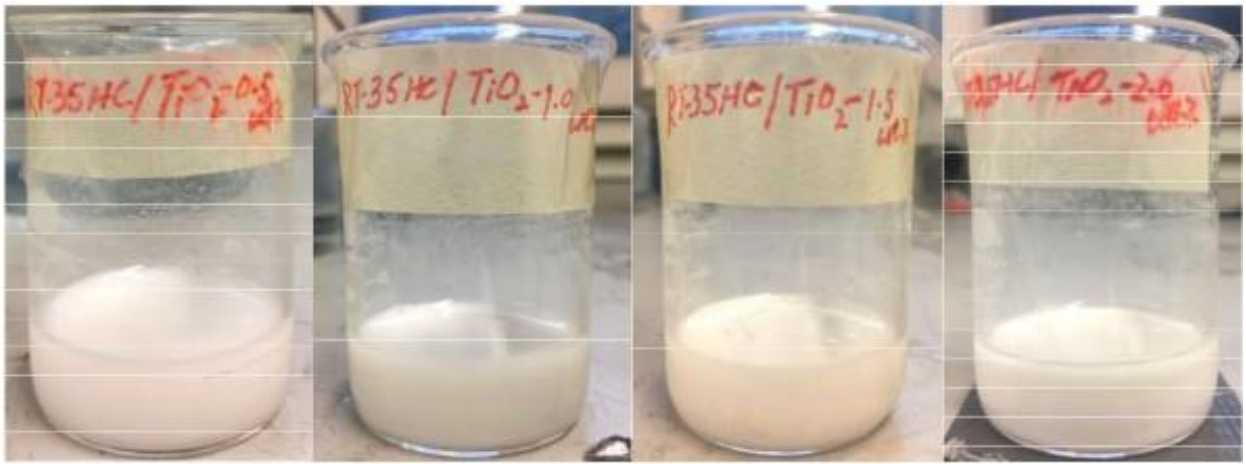

(a) (b) (c) (d)

Figure 2: *TiO_2 NCPCMs after sonication : (a) NCPCM1, (b) NCPCM2, (c) NCPCM3, (d) NCPCM4.*

3.1. Morphology and chemical interaction analysis

To visualize the surface morphology and elemental distribution of TiO_2 NPs in the NCPCMs, an environmental scanning electron microscopy (ESEM, FEI Quanta-650) was used along with energy-dispersive X–ray spectroscopy (EDS). To investigate the chemical composition of TiO_2 NPs and all samples, the fourier transfer infrared spectroscope (FITR, Bruker Tensor-27) at room temperature from $400 - 4000$ cm^{-1} range 4 cm^{-1} spectral res-

olution and accuracy of 0.01 cm'. The crystallographic analysis was analysed from X-ray powder diffraction (XRD) patterns TiO2 NPs and all samples, obtained with Bruker (D8-Advance, Bruker UK Limited) X-ray diffractometer with a monochromatic Cu-Ka radiation (A = 1.5406A) within 29 range of 5 - 60°.

3.2. Thermophysical properties analysis

To check the thermal stability and degradation temperature of NCPCMs, thermogravimetric analysis (TGA) and derivative thermogravimetry (DTG) were performed through SDT-Q600 simultaneous TGA/DSC having 0.1tig precision. A sample mass range of 5-8mg was placed in an aluminium pan and test was performed in range of 20 - 400°C with step rate of 10 °Cmin-1 under the N2 purging flow rate of 100 mL/min. The phase-transition temperatures and enthalpies of RT-35HC and NCPCMs were measured using differential scanning calorimeter (DSC-2500, TA instrument Inc., UK [46]) between temperature range of 10 - 50°C at a temperature rate of 1 °Cmin-1 in a pure N2 environment with ±0.04% accuracy and ±0.005°C precision. The specific heat capacity was measured from temperature range of 20 - 60°C at 3 °Cmin-1 constant heating rate by adopting Sapphire method. An aluminium Tzero Hermetic pan and lid was used filled with the sample mass around 3 - 5 mg precisely with no leakage. The thermal conductivity of pure RT-35HC and NCPCMs was measured using TCiTM thermal conductivity analyser (TCA) by C-Therm Technologies Ltd, Canada following the modified transient plane source (MTPS) method (ASTM no D7984) with the precision and accuracy better than 1% and 5%, respectively. The thermal conductivity was measured as a function of temperature ranging from 20 to 55 °C. Five readings were measured at constant temperature and an average value was considered with ±1.0% uncertainty. To take the thermographs to NCPCMs, infrared thermography (IRT) tests were performed over a IR thermographic camera (FLIR-SC2600-EA2). To provide a uniform heating, the samples were heated in a water pot on a hot plate.

4. Results and discussions

4.1. Morphological and elemental analysis

The ESEM scanning images, representing the micro-structural features and surface morphologies of TiO2 NPs and NCPCM4 shown in Figure 3. The spherical shape of TiO2 NPs can be seen from Figure 3a. Figure 3b and 3c represent the low vacuum secondary electron detector (LFD) and backscatter electron detector (BSED) images at 500 magnification for

low vacuum mode. Whereas, Figure 3d and 3e show the LFD and BSED of at 1000 magnification. It can be seen that TiO2 NPs are uniformly dispersed (white regions) over the surface of solid RT-35HC (dark regions) which is due the repulsive bonding of the SDBS acting as a surfactant. In addition, the homogeneous and heterogeneous percolation of TiO2 in RT-35HC can be observed in both of lower and higher magnifications. The presence of zones characterized by the heterogeneous aggregates of TiO2 NPs and zones of pure RT-35HC can be observed clearly. Similar observations of aggregation with Si02/A1203 nanoparticles had been reported by Chieruzzi et al. [47]. In the liquid phase of NCPCMs, solvation, "Brownian motion" and "electrostatic repulsion" cause the NPs to separate individually. However, this collision increases between the NPs by increasing the NPs concentration and Van der Waals force becomes stronger at a short range which results in the formation of aggregates and sedimentation of NPs at high concentration. Moreover, as the concentration increases, the density of NPs per unit area also increases which yields the more pathways for thermal transport in PCM [48]. The uniform dispersion and percolation of NPs depend on the size of the NPs. A better dispersion of NPs into PCMs can be achieved with smaller size of NPs.

The better understanding and visualization of NCPSMs, EDX maps of NCPCMs are shown in Figure 4. Figure 4a, 4b, and 4c which present the elemental distribution of carbon (C), oxygen (0) and titanium (Ti), respectively, of 2.0 wt.% of TiO2 NPs dispersed in RT-35HC. The red colour present in various zones of Figure 4a, shows the presence of C elements in RT-35HC, synthesized as a paraffin based PCM. Similarly, the cyan and green colours represent the aggregates of 0 and Ti elements present compound of TiO2 nanoparticles and RT-35HC PCM. The distribution of C, Ti and 0 in different colours can be illustrate in single image present in TiO2 dispersed NCPCM in Figure 5. It can be revealed that ESEM and EDX images show the agglomerated TiO2 NPs in difference zones of the NCPCM which correlate with the Ref [47]. Thus, the NPs with smaller size reveal the better dispersion into the PCM [49, 50].

4.2. Chemical composition analysis

The chemical composition and structural interaction of TiO2 NPs dispersed NCPCMs were verified by FTIR analysis. Figure 6 shows the transmittance band of FT-IR spectra of TiO2, RT-35HC and NCPCM1-4 between wave numbers of 500 and 4000 cm-1. The peaks around 510 and 526 cm-1 are attributed to the Ti-0 stretching vibrations in TiO2. For the

(a)

(b) (c)

(d) (e)

Figure 3: *ESEM images of (a)TiO2 NPs, NCPCM4 (b) LFD and (c) BSED at 500 magnification, (d) LFD and* (e) *BSED at 1000 magnification.*

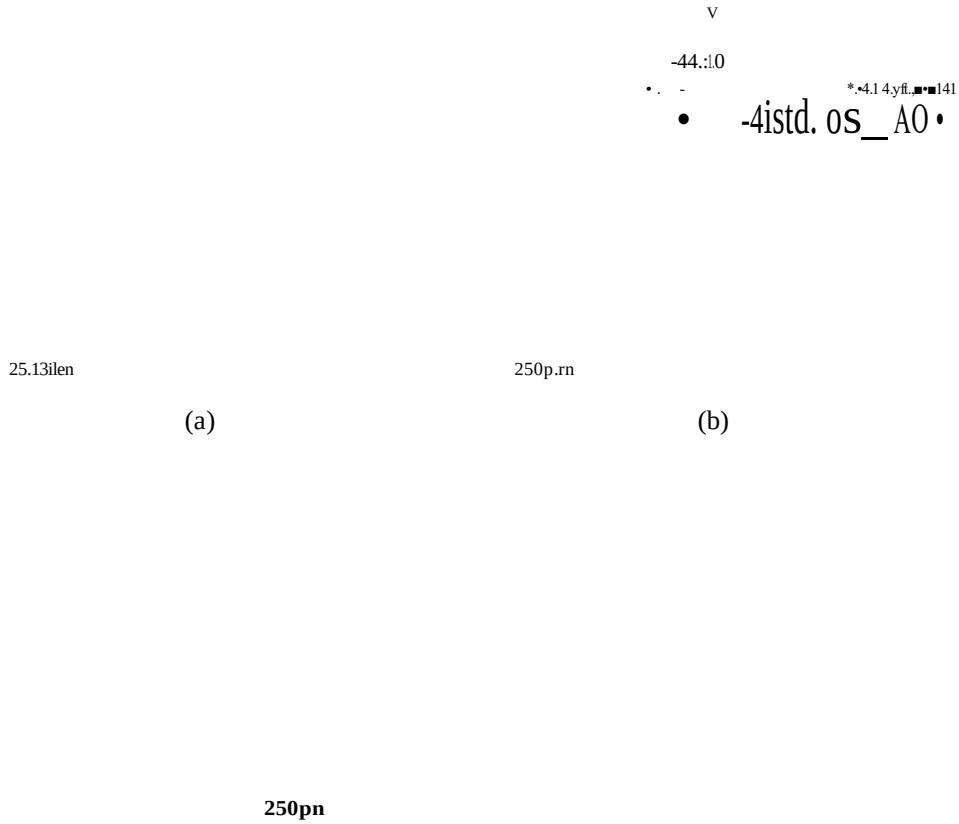

Figure 4: *EDX mapping of NCPCM4 (a) carbon-(red), (b) oxygen-(cyan), (c) Titanium-(green).*

Figure 5: *EDX map of Qxygen, Titanium, and carbon elements present in NCPCM4.*

spectrum of RT-35HC, it is observed that the three absorption bands at 2955, 2913, 2849 CM -1 assigned to medium C—H symmetrical and anti—symmetrical stretching vibration of methyl (—CH3) and methylene (—CH2—) groups. The scissoring of —CH2— appears at 1472

cm^{-1} and deformation of antisymmetric stretching vibration $-CH_3$ group in RT–35HC. A series of absorption bands at 1371, 1125, and 891 cm^{-1} attributed to the C–H bending and scissoring vibrations. A weak rocking vibration of C–H appears at 715 cm^{-1} in long-chain methyl group. No new peak is observed in NCPCM1–4 as revealed from FTIR results. More further, it can be seen that there is also no peak shift. Thus, there occurs no chemical reaction between the SDBS, TiO_2 and RT–35HC and only physical interaction is present.

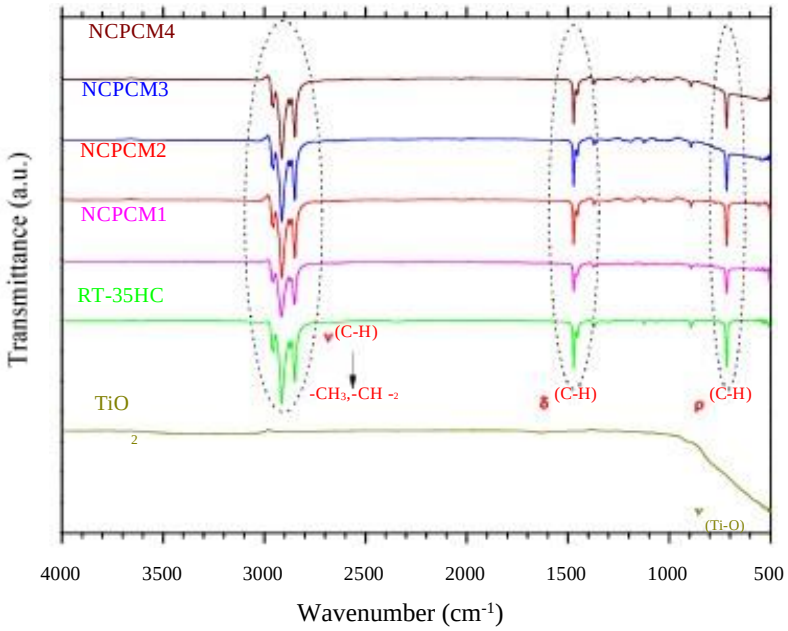

Figure 6: *FT-IR spectrum of TiO_2 and RT–35HC based NCPCMs.*

4.3. Crystallography analysis

The crystal structure and crystalline phase of TiO_2 NPs, RT–35HC and NCPCM1–4 were identified through XRD pattern and results were matched with the international centre for diffraction data (ICDD) database, as shown in Figure 7. The XRD diffraction of peaks of TiO_2 NPs at 2θ = 25.3°, 37.79°, 48.03°, 53.88° and 55.06° represent the lattice planes of (101), (004), (200), (105) and (211), respectively, which confirm the anatase form of the TiO_2 NPs with PDF No. 03-065-5714. The diffraction peaks of pure RT–35 was observed at 6.85° (002), 10.48° (003), 13.91° (004), 17.44° (005), 19.32° (010), 19.80° (011), 20.83° (012), 22.43° (013), 23.32° (105), 24.78° (-101), 25.65° (110), 28.12° (008), 31.75° (009), 34.75° (-110), 35.27° (0010), 39.83° (0-22), 42.73° (0012), 44.60° (207), 52.68° (220), 53.41° (-2-14) and 57.55° (-205) which attributed to the crystal planes of *n-eicosane* ($C_{20}H_{42}$) with PDF No. 00-045-1543. The physical presence of TiO_2 NPs can be found in NCPCMs such as at higher concentration of 2.0 wt.% of TiO_2 NPs are found at 25.34°, 39.62°, 47.74°, 54.81° and 56.00° which are well indexed as (101), (004), (200), (211) and (105), respectively, in

NCPCM4. Therefore, the XRD results of NCPCMs illustrate that dimensions of unit cell of RT–35HC crystal structure has not changed in NCPCMs and all the samples contain the peaks of TiO_2 NPs.

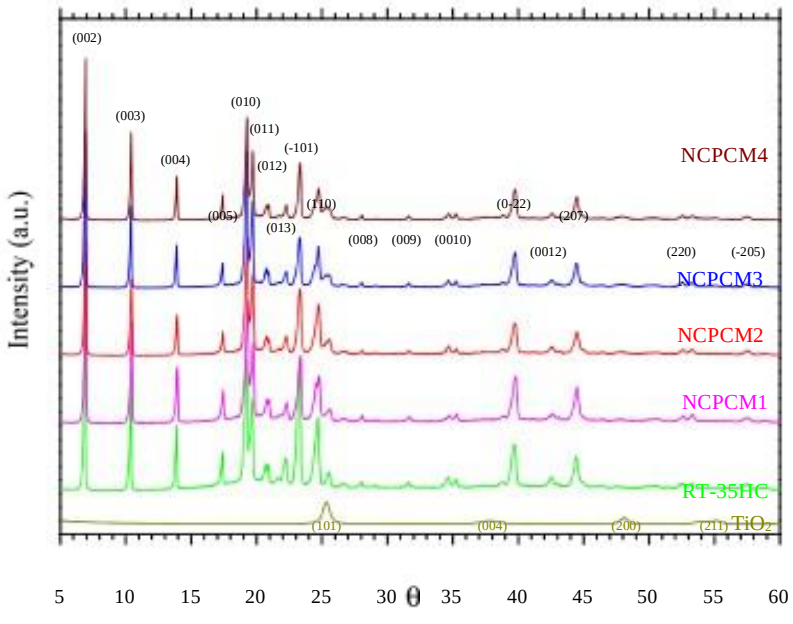

Figure 7: *XRD spectrum of TiO_2 and RT–35HC based NCPCMs*

4.4. Thermal stability analysis

Thermal stability analysis of pure RT-35HC and NCPCM1-4 are shown in Figure 8, conducted by TGA and DTG. The thermal stability was analysed depending upon the onset decomposition temperature (T_{onset}) of PCM degradation and rate of weight loss (R_{wl}). From figure 8a and 8b, it represent that a one–step and two–step thermal degradation processes are attributed to the TGA and DTG curves, respectively. The TGA curves show that there exists no weight loss distinguishably up to 120°C in any sample. The weight loss starts appearing with the rise of temperature and R_{wl} increases with further increase of temperature. For RT–35HC, the initial T_{onset} starts at 217.70°C and maximum degradation temperature ($T_{max.degradation}$) is 255.01°C with 1.85% residue (γ). The complete decomposition of RT–35HC is because of the evaporation which breakdown the hydrocarbon chain of RT–35HC into monomers (CH_3CH:$CH+CH_4$). From the results presented in Table 2 it has been observed that by increasing weight concentration of TiO_2, the initial T_{onset} also increases with a rise in γ content of the material. The γ concentration rises up to 3.79% in case of NCPCM4, which is maximum value among the given samples in Table 2. It can be seen from Figure 8 that NCPCM4 showed maximum thermal stability. It can be seen from that the thermal stability increase with the increase of weight concentration of TiO_2

in RT-35HC. This improved trend in thermal stability can be explained by the following reasons: (i) *the T_{onset} is related to the entire specific heat capacity (Cr) of Ti02/RT-35HC nanocomposites which can be raised by the Cp of TiO2 NPs, and* (ii) *enhanced thermal conductivity of NCPCMs which can transfer heat faster and uniformly within the PCM* [32]. In NCPCMs, the TiO2 NPs create the protective layer on the surface of pure RT-35HC which delay vaporization of RT-35HC during the thermal degradation. As NPs are likely to sediment which effect the thermal properties. Therefore, the DTG curves of NCPCM1-4 shown in 8b confirm that the dispersion NPs enhance the thermal stability of RT-35HC. Since, no decompositions in materials have been observed until ,,,150°C. So, hybrid can effectively be used for TM of electronic devices, Li-ion batteries and PV modules and TES applications.

Table 2: *Decomposition temperatures and residue of TiO2 and RT-35HC based NCPCMs.*

Sample	*Tonset* (°C)	*Tmax .degr adation (°C)*	*'Y (%)*
RT-35	217.70	255.01	1.85
NCPCM1	219.97	260.26	1.51
NCPCM2	226.77	263.55	1.96
NCPCM3	224.70	262.54	2.17
NCPCM4	223.50	262.29	3.79

4.5. Phase-change thermal properties analysis

The phase—change thermal properties of pure RT-35 and NCPCMs are determined using DSC for melting/cooling cycles, as shown in Figure 9. Figure 9a and 9b present the DSC thermographs of endothermic and exothermic curves, respectively and corresponding measured values of phase-transition temperatures and latent—heat of melting/cooling are summarized in Table 3. With the addition of TiO2 NPs, phase—changes thermal properties have slightly changed during the synthesizing process. Latent—heat of melting/solidifying of NCPCMs decreases by increasing the TiO2 NPs loadings. The pure RT-35HC and NCPCMs show the single endothermic peaks during melting which reflect an isomorphous crystalline form of RT-35HC either in pristine state or in composite state. On the other hand, it can be noticeably observed that pure RT-35 and NCPCMs show the bimodal crystallization behaviour by showing a main exothermic peak temperature along with an additional peak of higher temperature during solidification process. This two—phase transitions phenomenon can be explained due to the appearance of a metastable rotator phase prior to completing

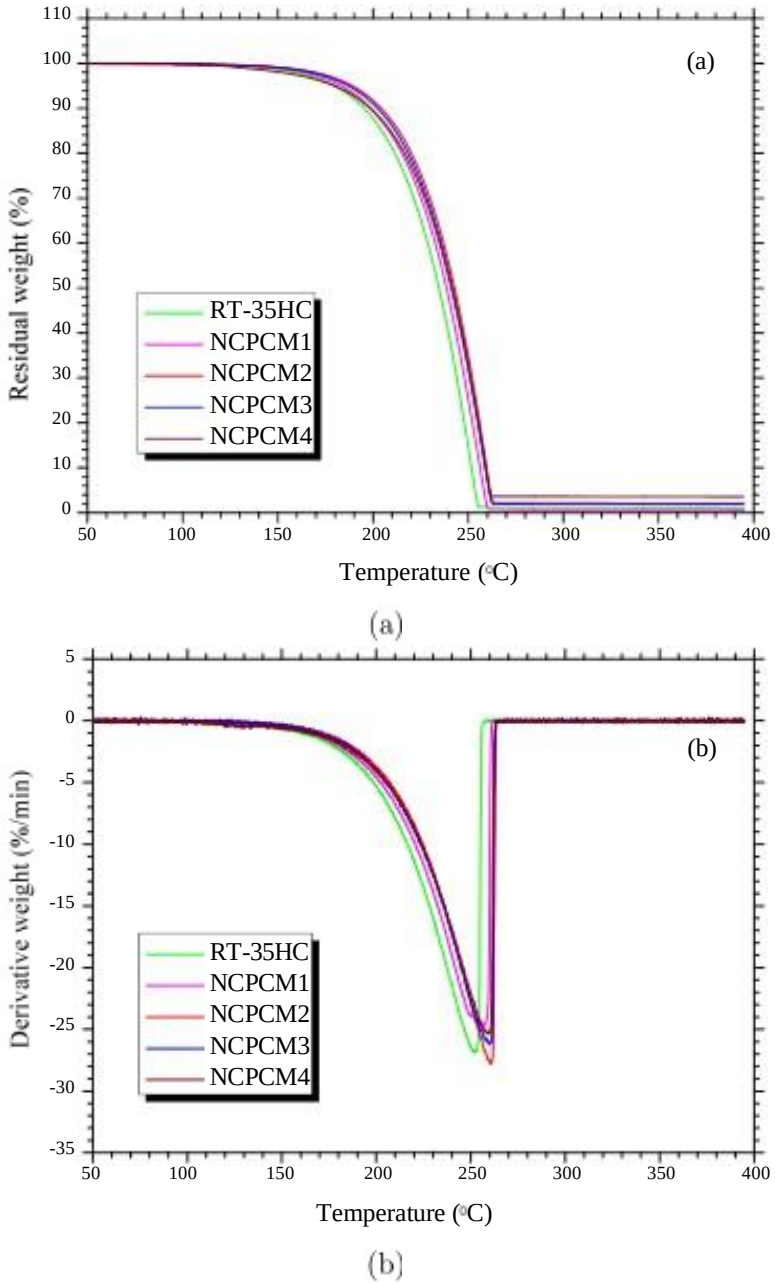

Figure 8: *(a) TGA and (b) DTG thermograms of TiO_2 and RT–35 based NCPCMs.*

the complete crystallization as a results of the heterogeneous nucleation during the cooling process, which has been mostly reported for the paraffin waxes [51, 52].

From the DSC results, the comparison of the melting (ΔH_m) and solidification (ΔH_s) enthalpies of pure RT-35HC and NCPCMs are presented in Figure 10. The ΔH_m and ΔH_s of pure RT-35HC are determined of 255.88 and 260.06 J/g, respectively. The reduction in ΔH_m of NCPCM1–4 has been obtained of 6.86%, 7.83%, 9.74% and 11.0% compared with RT–35HC. In similar way, the reduction in ΔH_s are obtained of 6.54%, 7.98%, 9.90% and 11.54% for NCPCM1–4, respectively. In comparison with RT–35HC, the maximum reduction ΔH_m and ΔH_s are obtained for NCPCM4 at 2.0 wt.% of TiO_2 which are 11.0% and

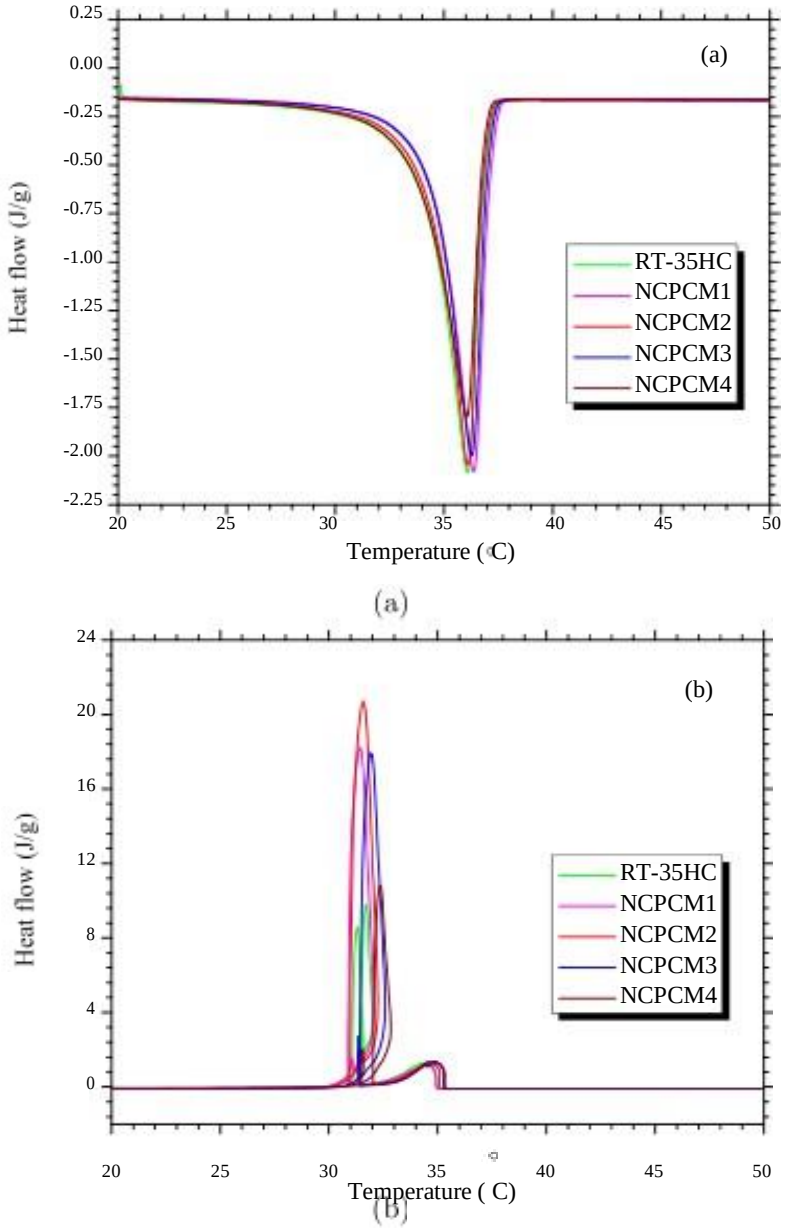

Figure 9: *DSC (a) Melting (b) Solidification curves of TiO_2 and RT–35HC based NCPCMs.*

11.54%, respectively, which is due to the addition of TiO_2 NPs. The Equation 1 is used to calculate the mass fraction (ω) of RT–35HC in crystallized form in NCPCMs, as follows:

$$\omega = \frac{\Delta H_{NCPCM}}{\Delta H_{PCM}} \times 100 \quad (1)$$

where, ΔH_{NCPCM} and ΔH_{PCM} are the endothermic latent–heat of NCPCM and pure PCM, respectively. During melting and solidification processes, the TiO_2 NPs replace the RT35–HC molecules resulting in reduce the latent–heat capacity of the NCPCM which lead to the absorption or release of more energy. The stronger the interaction between TiO_2 and RT35-HC, higher will be the latent–heat capacity of the NCPCM.

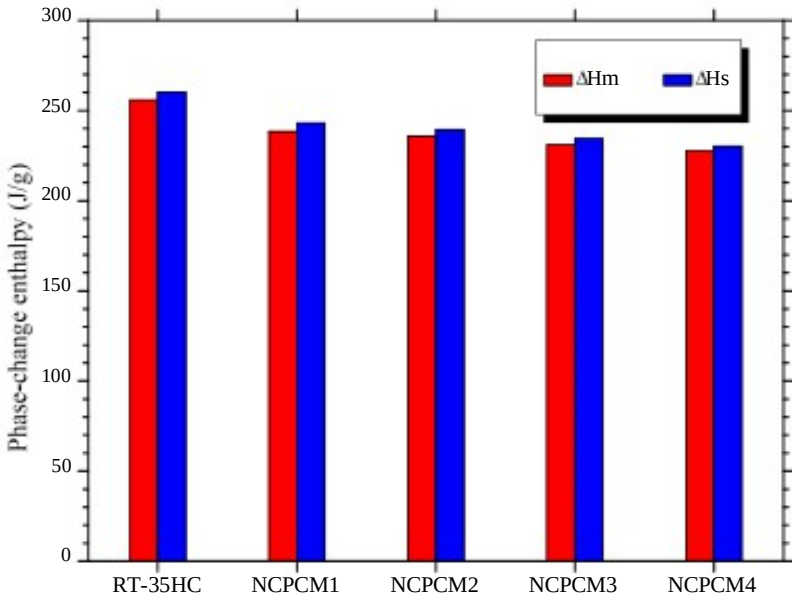

Figure 10: *Phase–change enthalpies of TiO_2 and RT–35HC based NCPCMs.*

Figure 11 illustrates the results of degree of super–cooling (ΔT) of pure RT–35HC and NCPCMs. The peak melting temperature (T_m) and crystallization temperature (T_c) of RT–35HC are determined as 36.09°C and 31.71°C, respectively. However, the slight variations are observed in T_c which are due the crystallization confinement of TiO_2 NPs surface layers within the NCPCMs. Furthermore, this interfacial surface layers cause to form the imperfect RT–35HC resulting in a slight variation in T_m. Thus, these factors cause to increase the ΔT. Maximum deviations in T_m are determined as -0.78%, -0.30%, -0.67% and 0.11% for NCPCM1–4, respectively, compared with the RT–35HC. Similar to this, by comparing with RT–3HC, the maximum deviations in T_c are found of 0.98%, 0.41%, -0.63% and 0.98% for NCPCM1–4, respectively. Furthermore, to achieve the crystallization point depression, heterogeneous nucleation can be acceptable by adding the TiO_2 NPs in RT–35HC [51]. However, it has been proved that higher difference in ΔT is an evidently disadvantageous to use the PCM for TM and TES applications. Since it can exhibt the hysteresis response during conjugate heat transfer.

The experimental and theoretical results of latent–heat of enthalpies of RT–35HC and NCPCMs are presented in Figure 12, calculated by the Equation 2 [53]:

$$\Delta L_{NCPCM} = \Delta L_{PCM} \cdot \omega = \Delta L_{PCM}(1 - \varphi) \tag{2}$$

where, φ and ω are the mass fraction of pure PCM and NPs, respectively. ΔL_{PCM} and ΔL_{NCPCM} are the experimental and theoretical latent–heat of enthalpies of pure PCM

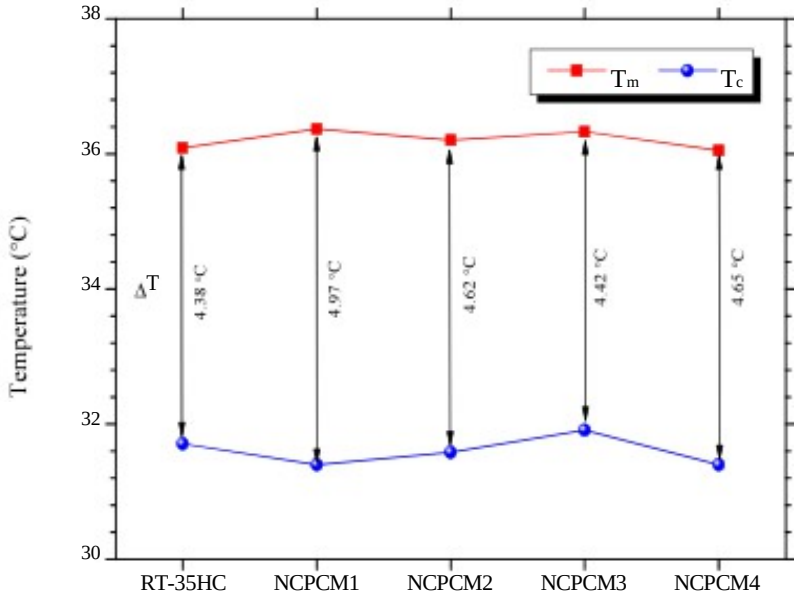

Figure 11: *Degree of super-cooling of TiO_2 and RT–35HC based NCPCMs.*

and NCPCM, respectively. The results reveal that experimental measurements of latent–heat of fusion are less than compared with the theoretical results, as shown in Figure 12. The relative error (RE) in experimental and theoretical values has been obtained 6 $\sim$ 9% for NCPCM1–4, given in Table 3. The similar trend of deviations in experimental and theoretical values latent–heat of fusion have reported in Refs. [26, 27, 53, 54]. The discrepancies in latent–heat values are because of the morphology, NPs size, shape, lattice structure and thermophysicla properties (i.e. density, surface area, specific heat and thermal conductivity etc.) of TiO_2 NPs in RT–35HC.

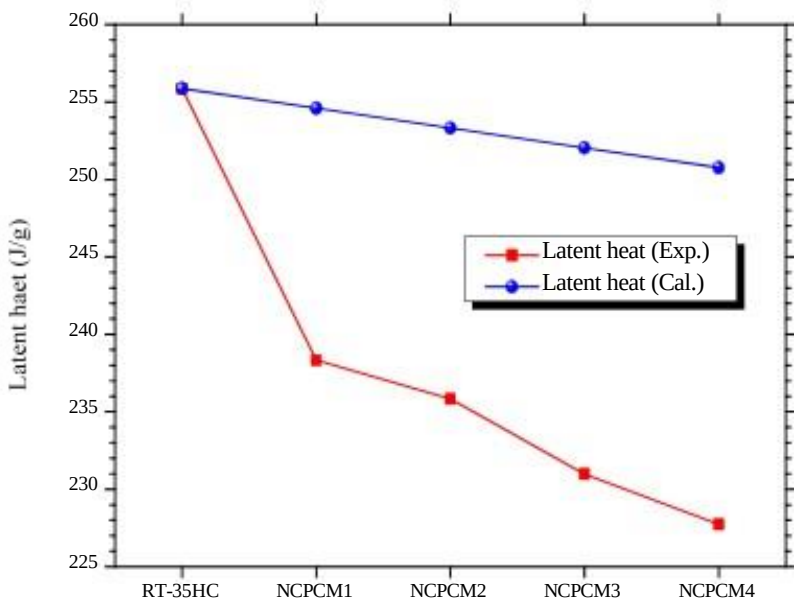

Figure 12: *Comparison of latent heats of TiO_2 and RT–35HC based NCPCMs.*

Table 3: *Thermal properties of TiO2 and RT-35HC based NCPCMs*.*

Sample	Melting					Solidification					w (%)	A T
	T oset,m	Tpeak,m	Allm,exp	Allm,cal	RE (%)	Toset,,	Tpeak,c	Alle,exp	*Allc,cal*	RE (%)		
RT-35	34.06	36.09	255.88	-	-	31.47	31.71	260.79	-	-	100	4.38
NCPCM1	34.46	36.37	238.33	254.60	6.39	31.99	32.05	243.04	258.76	6.08	93.14	4.32
NCPCM2	34.26	36.20	235.84	253.32	6.90	31.48	31.99	239.30	257.46	7.05	92.17	4.21
NCPCM3	34.44	36.33	230.97	252.04	8.36	30.95	31.58	234.32	256.16	8.53	90.26	4.75
NCPCM4	33.88	36.05	227.74	250.76	9.18	30.86	31.40	230.06	254.86	9.73	89.00	4.65

T oset,in: onset melting temperature, $T_{peak,m:}$ peak melting temperature, Alirri,exp: experimental latent-heat of melting, AH,,,,a/: calculated latent-heat of melting, To,,t,c: onset solidifying temperature, Tpeak,c: peak solidifying temperature, AH,,exp: experimental latent-heat of solidifying, AH,,,a/: calculated latent-heat of solidifying, RE: relative error, w: mass percentage of RT-35HC, AT: degree of super-cooling

304 4.*6. Thermal conductivity analysis*

305 The results of thermal conductivity variations and percentage enhancement of RT-35HC
306 and NCPCMs are illustrated in Figure 13 and 14, respectively, as function of temperature.
307 As expected, the increasing trend in thermal conductivity was achieved with the increase
308 of TiO2 NPs loading in NCPCMs for solid and liquid phases. For efficient and effective
309 TM, the thermal conductivity of the PCM contributed significantly in heat storage/release
310 rate while melting/cooling cycle. A PCM with lower thermal conductivity causes to mini-
311 mite the rate of total heat storage/release both in conduction and convection modes while
312 phase transformation. With the addition of TiO2 NPs, the maximum thermal conductivity
313 of 0.480 W/m.K was achieved at 2.0 wt.% of TiO2 and 35°C. The temperature range be-
314 tween 34 — 36°C is the phase—transition temperature range of pure RT-35HC at which the
315 NCPCMs are in metastable condition. The crystalline structure of the RT-35HC becomes
316 unstable and the increase in temperature accelerates the molecular vibration of in the lat-
317 tice, thus thermal conductivity of pure RT-35HC and NCPCMs increases dramatically at
318 the melting point (rs, 35°C) [31]. Figure 14 presents the average thermal conductivity of
319 solid—phase (20-30°C), phase—change (,--, 35°C) and liquid-phase (40-55°C) regions of pure
320 RT-35HC and NCPCM1-4. The constant trend in enhancement of thermal conductivity
321 was observed in solid and liquid phases. However a sharp increase and decrease trend was
322 observed when the temperature increased from 30°C to 35°C and then 35°C to 40°C, respec-
323 tively. Such deviations in results evidences that thermal conductivity of NCPCMs closely
324 depends on the operating temperature. This phenomenon was due to the random motion
325 of molecules within a disordered microstructure of lattice in liquid—phase. This molecular
326 motion collapse the percolation network established by NPs under the solid—phase [55]. The
327 thermal conductivities values of 0.333, 0.338 and 0.341 W/m.K are measured for NCPCM4
328 at temperature of 30°C, 25°C and 20°C, respectively, as shown in Figure 13. The relative
329 enhancement in effective thermal conductivities are obtained of 59.4%, 59.6% and 59.5%
330 at temperature of 30°C, 25°C and 20°C, respectively, for NCPCM4, as shown in Figure
331 14. The following Equation 3 was used to calculate the thermal conductivity enhancement
332 factor after dispersing the TiO2 NPs into the RT-35HC:

$$= \frac{kNCPCM — kpcm}{kpcm} \text{ x } 100 \qquad (3)$$

where, k_{PCM} and k_{NCPCM} are the thermal conductivity of pure PCM and the NCPCM, respectively.

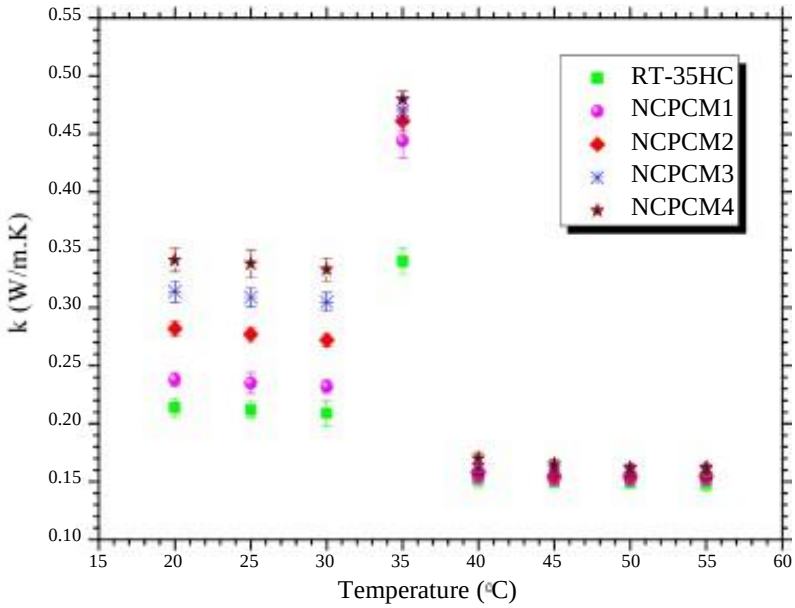

Figure 13: *Thermal conductivity of TiO_2 and RT–35HC based NCPCMs as a function of temperature.*

It can be seen from Figure 14 that thermal conductivity enhancement percentage increases linearly with increasing of TiO_2 loading both in solid and liquid phase. The maximum enhancement percentage of 11.4%, 31.9%, 46.9% and 59.5% for NCPCM1, NCPCM2, NCPCM3 and NCPCM4, respectively, at 20°C. In addition, Figure 15a and Figure 15b

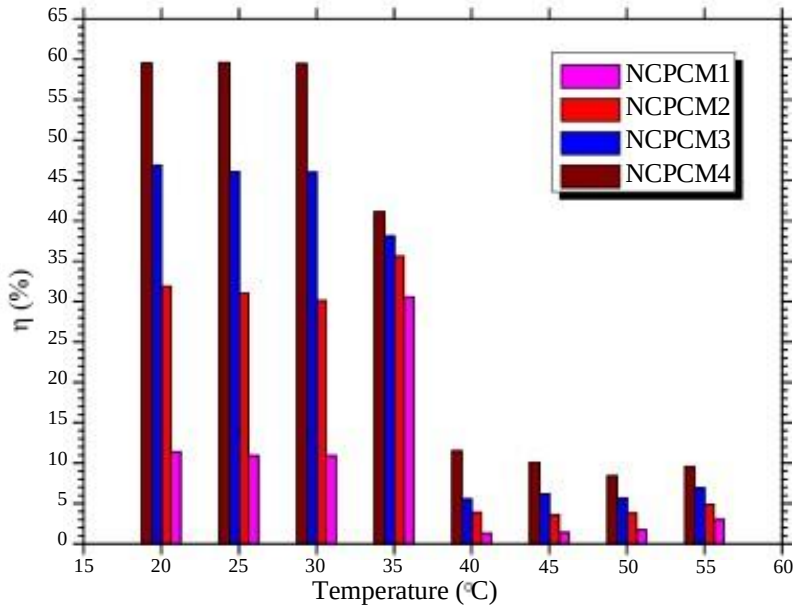

Figure 14: *Thermal conductivity enhancement of TiO_2 and RT–35HC based NCPCMs as a function of temperature.*

present the results of thermal conductivity ratio, a given by Equation 4:

$$= \frac{kNCPCM}{kpcm} \quad (4)$$

It can be revealed from that the value of e is greater than 1 which means that NCPCMs have the higher thermal conductivity than the pure PCM. In addition, higher values of e are obtained for NCPCMs having solid—phase compare to the liquid—phase. The correlations have been developed to predict the thermal conductivity of NCPCMs as a function of loading of nanoparticles for solid and liquid phases at temperature of 25°C and 55°C, respectively, as given below:

At 25°C:

$$kNCPCM = kpcm(0.31(p + 0.986) \quad (5)$$

At 55°C:

$$kNCPCM = \text{kpcm}(0.046\text{cp} + 1.003) \quad (6)$$

The enhancement mechanism of thermal conductivity of TiO2 nanoparticles in RT-35HC is shown Figure 16. At lower concentration of 0.5 wt.%, the TiO2 NPs well dispersed independently in the RT-35HC, which reduces the thermal interfacial resistance and enhance the heat flow, resulting in a slightly improvement of the thermal conductivity, as shown in Figure 16a. When the loading increases about 0.5 1.0 wt.%, a small part of TiO2 NPs are formed as clusters due to the intermolecular interaction between the small particles. These clusters are in favour of forming segmental thermal conductive networks which improve the heat transferring path, as shown in Figure 16b, and thus improve the thermal conductivity of NCPCMs. Further increasing the concentration of TiO2 from 1.0 — 2.0 wt.%, the NPs can easily be connected to build up the complete thermal conductive networks, as shown in Figure 16c and 16d, which lead to significant improvement in thermal conductivity [32].

4.7. *Specific heat capacity analysis*

Specific heat capacity (Cp) results of pure RT-35HC and NCPCMs are presented in Figure 17 from temperature range of 10 — 60°C to explore the results for solid and liquid phases. Since the Cp contributes less effect in total TES because of the lower TES density in

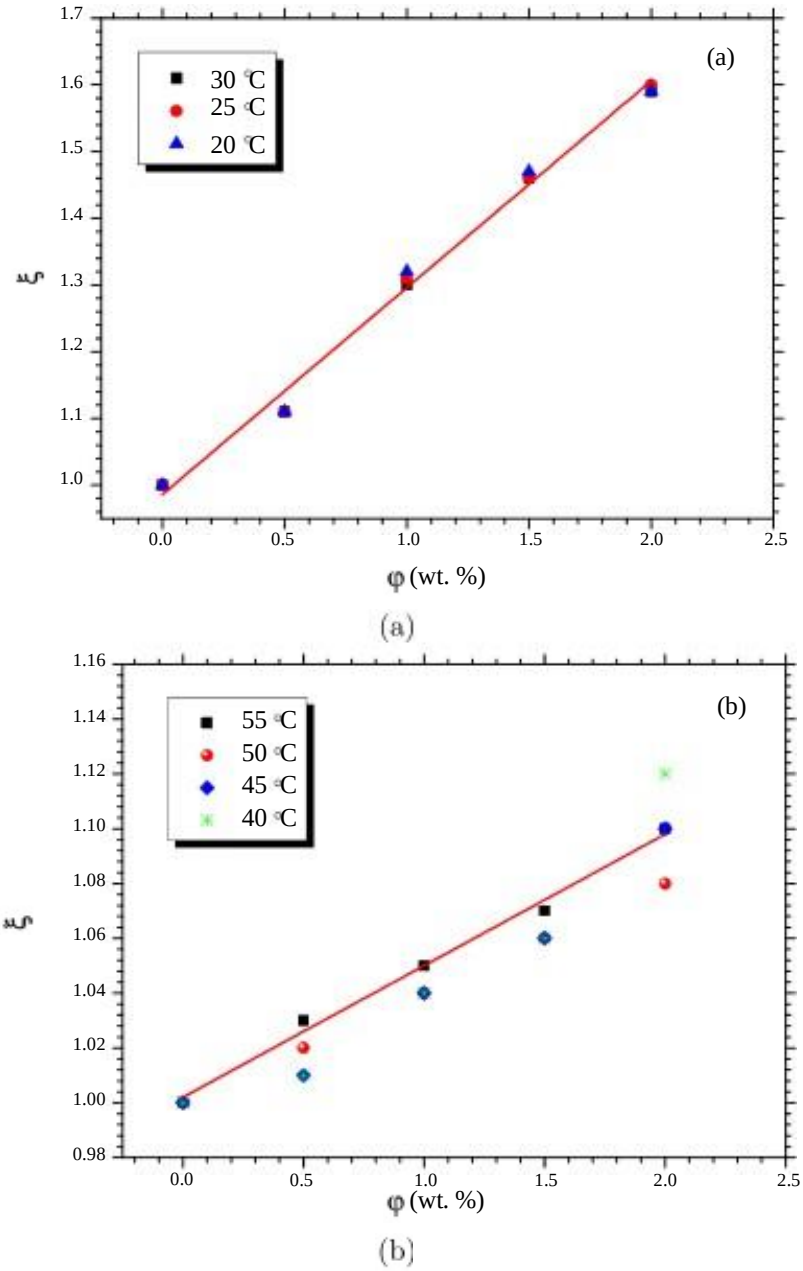

Figure 15: *Thermal conductivity ratios of TiO_2 and RT–35HC based NCPCMs as a function of temperature: (a) Solid-phase, (b) Liquid-phase.*

sensible heating storage. However, the additional effects are observed when PCM is applied in any TM and TES system along with the latent–heating storage. Thus, the comparison of C_p for solid and liquid phases of pure RT–35HC and NCPCMs are presented in Figure 17a and 17b, respectively. From Figure 17a, it can be illustrated that C_p of NCPCMs increases gradually with temperature from 14°C to 30°C in solid–phase, however, the constant trend is observed in liquid–phase. The present results of C_p of both phases showed the good agreement in variation of C_p with the previous studies [47, 56, 57]. It can been revealed from Figure 16 that the addition of TiO_2 NPs increase the C_p of pure PCM for both solid and

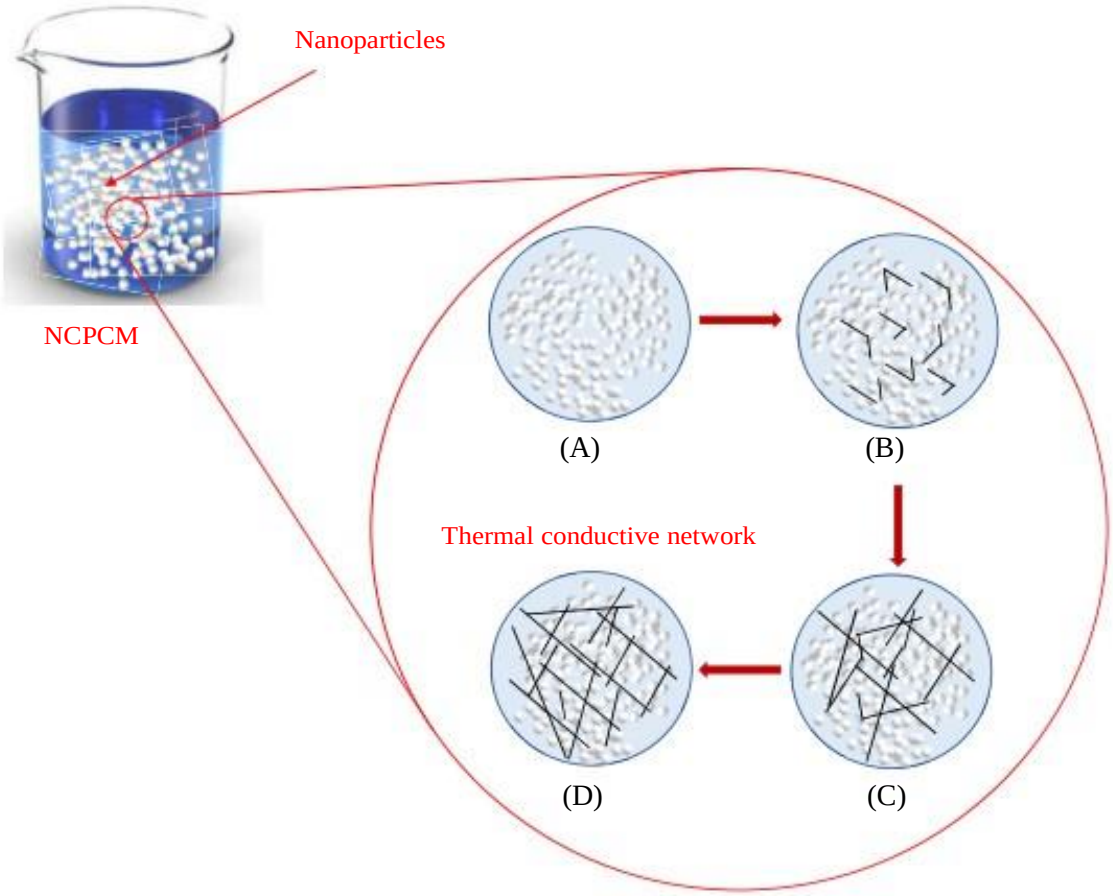

Figure 16: *Schematic representation of thermal conductive networks in TiO_2/RT–35HC NCPCMs with increasing loading of TiO_2: (a)* 0.5 *wt.%, (b)* 1.0 *wt.%, (c)* 1.5 *wt.%, (d)* 2.0 *wt.%.*

liquid phases as the weight percentage increases. For solid and liquid phases, the C_p values of pure RT–35HC are measured of 1.88 and 1.77 J/g.°C, respectively. The higher values of C_p are obtained of 2.84 and 2.56 J/g.°C at 25°C and 50°C, respectively, for NCPCM4. The polynomial equations are generated for solid phase from 14°C to 30°C for each NCPCM1–4 after fitting the experimental data, mentioned in Equation 7 and coefficients are given in Table 4.

$$C_P = AT^3 + BT^2 + CT + D \tag{7}$$

Figure 18 illustrates the comparison of C_p for pure RT–35HC and NCPCM1–4 for 25°C and 50°C to report the data for solid and liquid phases. It can be seen that with the increase of the TiO_2 loading, C_p increases for both solid and liquid phases and the maximum enhancements are obtained of 50.90% and 44.55%, respectively, for solid and liquid phases NCPCM4 compared with the pure RT–35HC. The C_p enhancement factor (ζ) is calculated

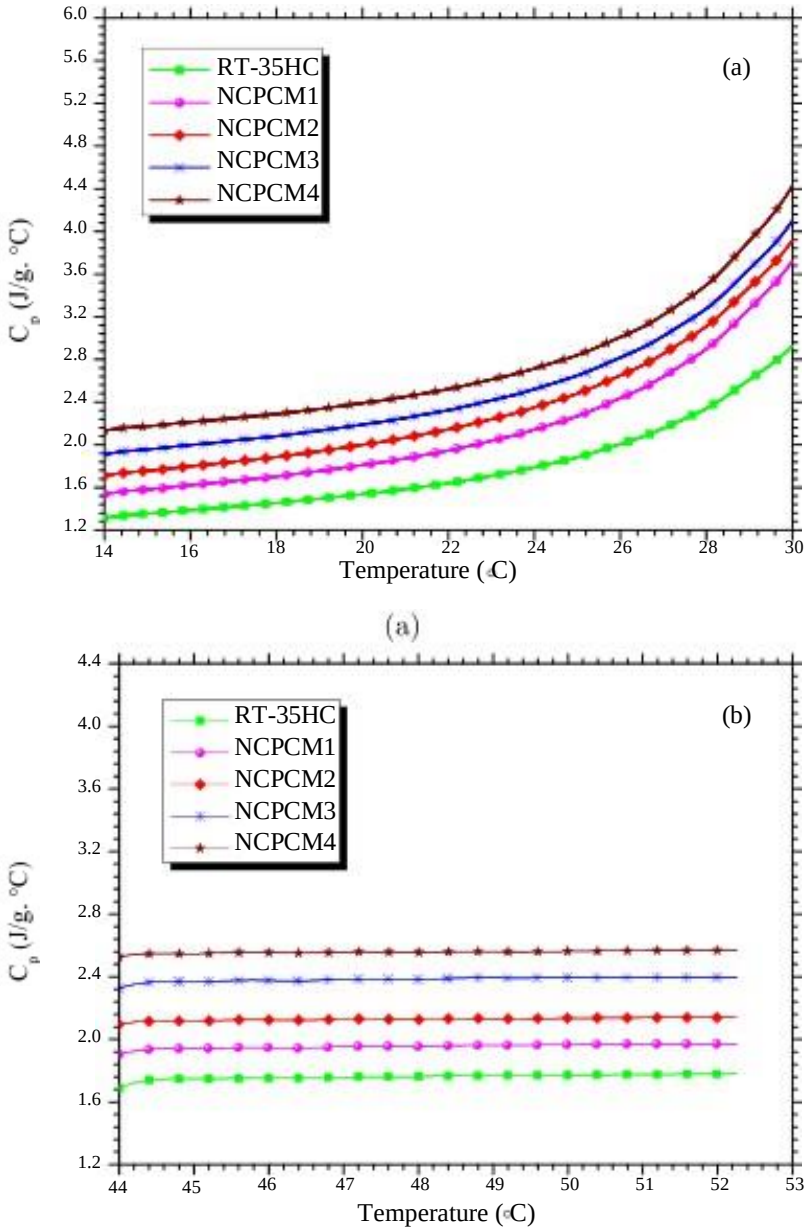

Figure 17: *C_p curves of pure RT–35HC and NCPCMs: (a)-solid–phase (b) liquid–phase.*

by using Equation 8 to evaluate the NPs effect in heat transfer rate, as follows:

$$\zeta = \frac{C_{P_{NCPCM}} - C_{P_{PCM}}}{C_{P_{PCM}}} \times 100 \tag{8}$$

where, $C_{P_{NCPCM}}$ and $C_{P_{PCM}}$ are the C_p of the NCPCM and PCM, respectively.

The enhancement in C_p is associated with the following reasons: (i) an enhanced anharmonicity of the atomic interaction due to their volume expansion, (ii) impurities [58], (iii) the grain boundaries of nanosized materials which possess an excess volume with respect to the perfect crystal lattice and (iv) the high specific surface energies related to the high sur-

Table 4: *Coefficients of the third-order polynomials in solid-state,* G *(J/g.° C).*

	A	B	C	D	R2
RT-35	0.0006	-0.0349	0.6687	-2.9832	0.9988
NCPCM1	0.0009	-0.0493	0.9384	-4.4479	0.9984
NCPCM2	0.0008	-0.0457	0.8701	-3.8549	0.9987
NCPCM3	0.0009	-0.0489	0.9319	-4.0415	0.9985
NCPCM4	0.0011	-0.0583	1.1128	-4.9497	0.9974

face area of the NPs per unit volume [59, 60]. Theoretically, the Cp of materials is directly related to crystal structure, or its vibrational and configurational entropy which significantly affected by the nearest-neighbour configurations. Nanosized materials are structurally characterized by the metastable grain boundaries in which the nearest-neighbour configurations are much different from the coarse-grained state [60].

In addition, the morphology of NPs also influences significantly, since the smaller size NPs provide the larger interfacial surface area per unit mass between solid NPs and surrounding material, thus increase the contribution of interfacial effects in the suspension [61, 62, 63]. The interfacial interaction of solid-solid or solid-liquid may alter phonon spectrum or phonon vibration mode of NPs near the surface area and therefore, change the $_{Cp}$ of NCPCM [64]. The high specific surficial interface area of NPs can adsorb liquid molecules $_{to}$ its surface which form the liquid layers. These liquid layers constrain the NPs and alter their free-boundary surface atoms into the non-free interior atoms [59, 64]. Therefore, the variation in Cp of NCPCMs is because of the varied Gibbs free energy of the NPs and liquid layers.

4.8. Infrared thermography analysis

The thermographics images of NCPCM1-4 are presented in Figure 19 to visualize the surface temperature distribution at different time interval from 5 to 30 min at a constant base temperature of hot-plate. The melting phenomenon of NCPCMs with different loadings of TiO2 can be seen clearly for each time step. There is a clear difference in temperature between the samples and background due to the latent-heat absorption of NCPCMs during phase-transition. The change in colours from blue to red are showing the range of temperature from lower to higher because of constant heating. The thermographic images reflect the real time uniform surface temperature distribution of NCPCMs and uniform melting of each sample can be observed during heating. The quick flow away and melting of NCPCMs were observed as the loading of TiO2 increase from 0.5 to 2.0wt.%, as shown in Figure 19c.

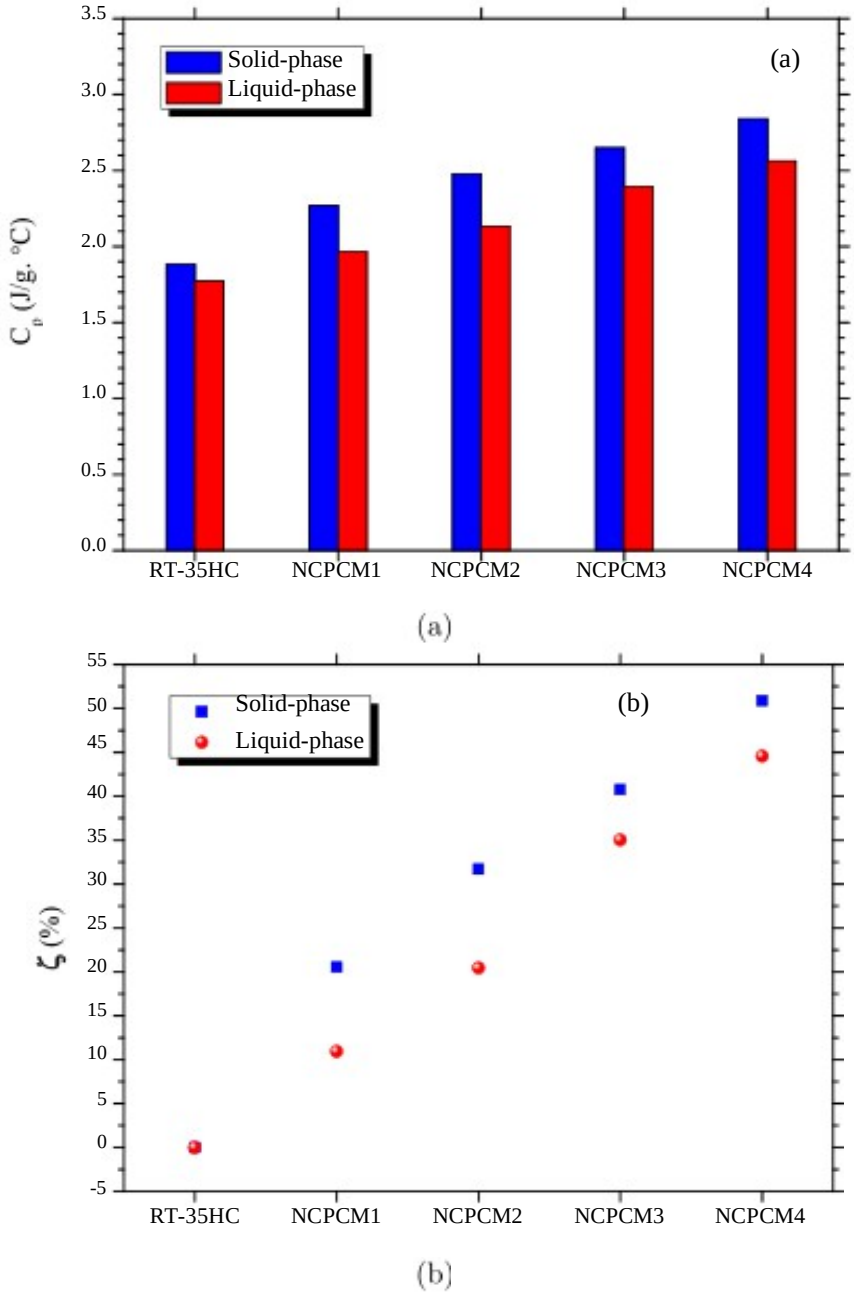

Figure 18: *(a) Comparison of C_p curves and (b) specific heat capacity enhancement of pure RT–35HC and NCPCMs.*

While solid–liquid phase transformation, the NCPCMs experienced the uniform natural convection heat transfer enhancement. Figure 19d shows the complete melting NCPCM3 and NCPCM4 occurs at 20 min whereas the temperature variations, reflected from colours, show that NCPCM4 has the higher temperature compared to NCPCM3. The reason behind is that NCPCM4 has the higher concentration of TiO_2 which increases the heat transfer rate results in reduces the melting time of NCPCM4. In addition, thermographic images show the uniform melting process which is due the homogeneous dispersion of TiO_2 NPs in RT–35HC, resulting in improve the heat absorption/dissipation rate for TM and TES

applications.

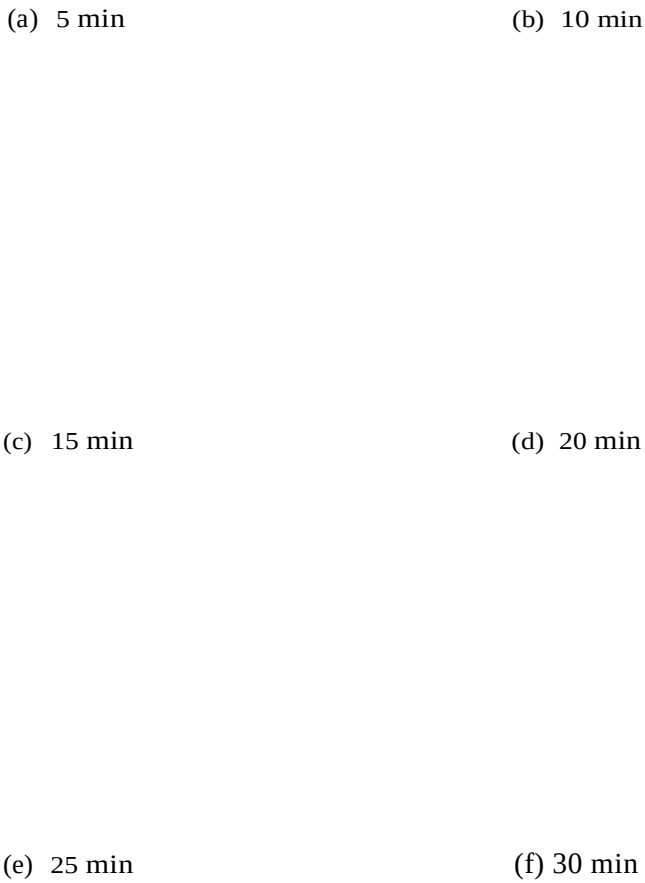

Figure 19: *Infrared thermography images of the melting process of NCPCM1-(A), NCPCM2-(B), NCPCM3-(C) and NCPCM4-(D): at different time steps with temperature variation in °C.*

5. Conclusions

The current experimental study investigated the chemical, physical and thermal properties of TiO2 dispersed nanocomposite phase change materials (NCPCMs) of varying loading into the RT-35HC. The chemical, physical and thermal properties of NCPCMs were determined by various material characteristic techniques such as ESEM, FT—IR, TGA, DCS

and thermal conductivity analyser to explore the best NCPCM for efficient TM and TES applications. The key findings are summarized as follows:

- The ESEM and XRD results revealed that uniform dispersion of TiO2 nanoparticles into RT-35HC. The presence of TiO2 nanoparticles in pure RT-35HC was observed through surface morphological and crystallography analysis.

- The FT—IR spectrum revealed that there is no chemical interaction of TiO2 nanoparticles with RT-35HC and there is only physical interaction of TiO2 with RT-35HC.

- The TGA and DTG results show that all NCPCMs have good thermal and chemical stability. With the addition of TiO2 improved the thermal and chemical stability of pure RT-35HC.

- The latent—heat of fusion was decreased with increasing the loading of TiO2. The optimum values of latent heat of 235.84 J/g at 1.0 wt.% of corresponding thermal conductivity of 0.284 W/m.K. In addition maximum deviation in latent heat and peak melting temperature were observed of 11.0% and 0.11%, respectively, at 2.0 wt.% of TiO2.

- The maximum thermal conductivities were obtained at phase-transition temperature of 0.444, 0.461, 0.471 and 0.480 W/m.K for NCPCM1-4, respectively. However, higher thermal conductivity of 0.341 W/m.K was obtained in solid—phase of corresponding thermal conductivity enhancement percentage of 59.5% at 2.0 wt.% of TiO2 compared to the pure RT-35HC.

- The addition of the TiO2 nanoparticles increases the specific heat capacity of the pure PCM for both solid and liquid phases. Furthermore, specific heat capacity of NCPCMs increases with the increase of the TiO2 mass concentrations. The higher values of specific heat capacities were obtained as 2.84 and 2.56 J/g.°C at 25°C and 50°C, respectively, at 2.0 wt.% of TiO2 compared to the pure RT-35HC.

- The uniform melting and temperature distribution were observed from IR thermographic images which revealed that with the increase of TiO2 mass concentrations heat transfer rate increases.

It can be concluded from the presented results that newly developed Ti02/RT-35HC base nanocomposite PCMs presented acceptable improvement in TES properties and efficient

phase—change heat transfer characteristics. Thus, these nanocomposite PCMs have significant potential in passive TM systems for electronic devices, Li—ion batteries, photovoltaic modules and direct utilization in solar thermal energy storage.

6. Acknowledgement

This research is facilitated by the Faculty of Engineering, University of Nottingham, UK research infrastructure. The corresponding author (Adeel Arshad) acknowledges the University of Nottingham for awarding him the *Faculty of Engineering Research Excellence PhD Scholarship* to pursue a Ph.D. research program. The authors acknowledge the use of facilities at Nanoscale and Microscale Research Centre of the University of Nottingham supported by Engineering and Physical Sciences Research Council [grant number EP/L022494/1].

References

[1] M. A. Bashir, A. Giovannelli, K. P. Amber, M. S. Khan, A. Arshad, A. M. Daabo, High-temperature phase change materials for short-term thermal energy storage in the solar receiver: Selection and analysis, Journal of Energy Storage 30 (2020) 101496. doi:10.1016/j.est.2020.101496.

[2] A. R. M. Siddique, S. Mahmud, B. Van Heyst, A comprehensive review on a passive (phase change materials) and an active (thermoelectric cooler) battery thermal management system and their limitations, Journal of Power Sources 401 (2018) 224-237.

[3] H. M. Ali, A. Arshad, Experimental investigation of n-eicosane based circular pin-fin heat sinks for passive cooling of electronic devices, International Journal of Heat and Mass Transfer 112 (2017) 649-661. doi:10.1016/j.ijheatmasstransfer.2017.05.004.

[4] R. Gulfam, P. Zhang, Z. Meng, Advanced thermal systems driven by paraffin-based phase change materials — a review, Applied Energy 238 (2019) 582-611. doi :10.1016/apenergy 2019.01.114.

[5] H. Faraji, M. Faraji, M. E. Alami, Y. Hariti, A. Arshad, A. Hader, A. Benkaddour, Cooling of recent microprocessors by the fusion of nano-enhanced phase change materials, Materials Today: Proceedingsdoi : 10.1016/j . matpr . 2020.04.342.

[6] D. C. Hyun, N. S. Levinson, U. Jeong, Y. Xia, Emerging applications of phase-change materials (PCMs): Teaching an old dog new tricks, Angewandte Chemie International Edition 53 (15) (2014) 3780-3795. doi : 10.1002/anie . 201305201.

[7] A. J. Carrillo, J. Gonzalez-Aguilar, M. Romero, J. M. Coronado, Solar energy on demand: A review on high temperature thermochemical heat storage systems and materials, Chemical reviews 119 (7) (2019) 4777-4816.

[8] A. Arshad, H. M. Ali, W.-M. Yan, A. K. Hussein, M. Ahmadlouydarab, An experimental study of enhanced heat sinks for thermal management using n-eicosane as phase change material, Applied Thermal Engineering 132 (2018) 52-66. doi: 10.1016/j.applthermaleng.2017.12.066.

[9] H. M. Ali, A. Arshad, M. Jabbal, P. Verdin, Thermal management of electronics devices with PCMs filled pin-fin heat sinks: A comparison, International Journal of Heat and Mass Transfer 117 (2018) 1199-1204. doi:10.1016/j.ijheatmasstransfer.2017.10 . 065.

[10] J. M. Mandi, S. Lohrasbi, E. C. Nsofor, Hybrid heat transfer enhancement for latent-heat thermal energy storage systems: A review, International Journal of Heat and Mass Transfer 137 (2019) 630-649. doi:10.1016/j.ijheatmasstransfer.2019.03.111.

[11] A. Arshad, M. Jabbal, P. T. Sardari, M. A. Bashir, H. Faraji, Y. Yan, Transient simulation of finned heat sinks embedded with PCM for electronics cooling, Thermal Science and Engineering Progress 18 (2020) 100520. doi:10.1016/j. tsep .2020.100520.

[12] X. Yang, Z. Niu, Q. Bai, H. Li, X. Cui, Y.-L. He, Experimental study on the solidification process of fluid saturated in fin-foam composites for cold storage, Applied Thermal Engineering 161 (2019) 114163. doi:10.1016/j.applthermaleng.2019.114163.

[13] X. Huang, X. Chen, A. Li, D. Atinafu, H. Gao, W. Dong, G. Wang, Shape-stabilized phase change materials based on porous supports for thermal energy storage applications, Chemical Engineering Journal 356 (2019) 641-661. doi: 10.1016/j . cej .2018. 09.013.

[14] M. M. Umair, Y. Zhang, K. Iqbal, S. Zhang, B. Tang, Novel strategies and supporting materials applied to shape-stabilize organic phase change materials for thermal energy storage—a review, Applied Energy 235 (2019) 846-873. doi :10.1016/j . apenergy .. 2018.11.017.

[15] A. N. Keshteli, M. Sheikholeslami, Nanoparticle enhanced PCM applications for intensification of thermal performance in building: A review, Journal of Molecular Liquids 274 (2019) 516-533. doi: 10.1016/j .molliq.2018.10.151.

[16] K. Y. Leong, M. R. A. Rahman, B. A. Gurunathan, Nano-enhanced phase change materials: A review of thermo-physical properties, applications and challenges, Journal of Energy Storage 21 (2019) 18-31. doi :10.1016/j . est .2018.11.008.

[17] K. W. Shah, A review on enhancement of phase change materials - a nanomaterials perspective, Energy and Buildings 175 (2018) 57-68. doi:10.1016/j.enbuild.2018. 06.043.

[18] W. Aftab, X. Huang, W. Wu, Z. Liang, A. Mahmood, R. Zou, Nanoconfined phase change materials for thermal energy applications, Energy & Environmental Science 11 (6) (2018) 1392-1424. doi:10.1039/c7ee03587j.

[19] A. Arshad, M. Jabbal, Y. Yan, J. Darkwa, The micro-/nano-pcms for thermal energy storage systems: A state of art review, International Journal of Energy Research 43 (11) (2019) 5572-5620. arXiv:https://onlinelibrary.wiley.com/doi/pdf/10.1002/er.4550, doi:10.1002/er.4550.
URL https://onlinelibrary.wiley.com/doi/abs/10.1002/er.4550

[20] C. Liu, Z. Rao, J. Zhao, Y. Huo, Y. Li, Review on nanoencapsulated phase change materials: Preparation, characterization and heat transfer enhancement, Nano Energy 13 (2015) 814-826. doi:10.1016/j.nanoen.2015.02.016.

[21] F. Rodriguez-Cumplido, E. PabOn-Gelves, F. Chejne-Jana, Recent developments in the synthesis of microencapsulated and nanoencapsulated phase change materials, Journal of Energy Storage 24 (2019) 100821. doi:10.1016/j.est.2019.100821.

[22] E. M. Shchukina, M. Graham, Z. Zheng, D. G. Shchukin, Nanoencapsulation of phase change materials for advanced thermal energy storage systems, Chemical Society Reviews 47 (11) (2018) 4156-4175. doi:10.1039/c8cs00099a.

[23] L. Qiu, N. Zhu, Y. Feng, E. E. Michaelides, G. Zyla, D. Jing, X. Zhang, P. M. Norris, C. N. Markides, 0. Mahian, A review of recent advances in thermophysical properties at the nanoscale: From solid state to colloids, Physics Reportsdoi: 10.1016/j.physrep.2019.12.001.

[24] S. Akin, S. Sonmezoglu, Metal oxide nanoparticles as electron transport layer for highly efficient dye-sensitized solar cells, in: Emerging Materials for Energy Conversion and Storage, Elsevier, 2018, pp. 39-79. doi:10.1016/b978-0-12-813794-9.00002-8.

[25] M. Bashar, K. Siddiqui, Experimental investigation of transient melting and heat transfer behavior of nanoparticle-enriched PCM in a rectangular enclosure, Journal of Energy Storage 18 (2018) 485-497. doi:10.1016/j.est.2018.06.006.

[26] X. Li, Y. Zhou, H. Nian, X. Zhang, 0. Dong, X. Ren, J. Zeng, C. Hai, Y. Shen, Advanced nanocomposite phase change material based on calcium chloride hexahydrate

with aluminum oxide nanoparticles for thermal energy storage, Energy & Fuels 31 (6) (2017) 6560-6567. doi:10. 1021/acs energyfuels 7b00851.

[27] R. Sharma, P. Ganesan, V. Tyagi, H. Metselaar, S. Sandaran, Thermal properties and heat storage analysis of palmitic acid-TiO 2 composite as nano-enhanced organic phase change material (NEOPCM), Applied Thermal Engineering 99 (2016) 1254-1262. doi:10.1016/j.applthermaleng.2016.01.130.

[28] S. Sami, N. Etesami, Improving thermal characteristics and stability of phase change material containing tio2 nanoparticles after thermal cycles for energy storage, Applied Thermal Engineering 124 (2017) 346-352.

[29] T.-P. Teng, C.-C. Yu, Characteristics of phase-change materials containing oxide nano-additives for thermal storage, Nanoscale Research Letters 7 (1). doi : 10.1186/ 1556-276x-7-611.

[30] J. Wang, H. Xie, Z. Guo, L. Guan, Y. Li, Improved thermal properties of paraffin wax by the addition of TiO2 nanoparticles, Applied Thermal Engineering 73 (2) (2014) 1541-1547. doi : 10.1016/j . applthermaleng 2014.05.078.

[31] S. Motahar, N. Nikkam, A. A. Alemrajabi, R. Khodabandeh, M. S. Toprak, M. Muhammed, Experimental investigation on thermal and rheological properties of n-octadecane with dispersed tio2 nanoparticles, International Communications in Heat and Mass Transfer 59 (2014) 68-74.

[32] Y. Chen, W. Luo, J. Wang, J. Huang, Enhanced thermal conductivity and durability of a paraffin wax nanocomposite based on carbon-coated aluminum nanoparticles, The Journal of Physical Chemistry C 121 (23) (2017) 12603-12609. doi:10.1021/acs. jpcc.7b02651.

[33] M. Nourani, N. Hamdami, J. Keramat, A. Moheb, M. Shahedi, Thermal behavior of paraffin-nano-a12o3 stabilized by sodium stearoyl lactylate as a stable phase change material with high thermal conductivity, Renewable Energy 88 (2016) 474-482. doi: 10.1016/j.renene.2015.11.043.

[34] M. Nourani, N. Hamdami, J. Keramat, A. Moheb, M. Shahedi, Preparation of a stable nanocomposite phase change material (NCPCM) using sodium stearoyl lactylate (SSL)

as the surfactant and evaluation of its stability using image analysis, Renewable Energy 93 (2016) 404-411. doi :10.1016/j . renene . 2016.02.073.

[35] A. Babapoor, G. Karimi, S. Sabbaghi, Thermal characteristic of nanocomposite phase change materials during solidification process, Journal of Energy Storage 7 (2016) 74-81. doi :10.1016/j . est .2016.05.006.

[36] A. Babapoor, G. Karimi, Thermal properties measurement and heat storage analysis of paraffinnanoparticles composites phase change material: Comparison and optimization, Applied Thermal Engineering 90 (2015) 945-951. doi : 10. 1016/j . applthermaleng. 2015.07.083.

[37] Y. Pahamli, M. Hosseini, A. Ranjbar, R. Bahrampoury, Effect of nanoparticle dispersion and inclination angle on melting of PCM in a shell and tube heat exchanger, Journal of the Taiwan Institute of Chemical Engineers 81 (2017) 316-334. doi:10.1016/j.jtice.2017.09.044.

[38] B. Praveen, S. Suresh, Experimental study on heat transfer performance of neopentyl glycol/CuO composite solid-solid PCM in TES based heat sink, Engineering Science and Technology, an International Journal 21 (5) (2018) 1086-1094. doi :10.1016/j . jestch.2018.07.010.

[39] A. R. M. Siddique, S. Mahmud, B. V. Heyst, A comprehensive review on a passive (phase change materials) and an active (thermoelectric cooler) battery thermal management system and their limitations, Journal of Power Sources 401 (2018) 224-237. doi:10.1016/j.jpowsour.2018.08.094.

[40] S. K. Sahoo, M. K. Das, P. Rath, Application of TCE-PCM based heat sinks for cooling of electronic components: A review, Renewable and Sustainable Energy Reviews 59 (2016) 550-582. doi :10.1016/j . rser .2015.12.238.

[41] Titanium (iv) oxide, anatase sigma-aldrich, inc. uk, accessed: 01/10/2019. URL https : //www. sigmaaldrich. com/catalog/product/aldrich/637254?lang=en&region=GB

[42] Sodium dodecylbenzene sulfonate, sigma-aldrich, uk, accessed: 01/10/2019. URL https : //www. sigmaaldrich. com/catalog/product/aldrich/289957?lang=en&region=GB

[43] A. Arshad, M. Jabbal, Y. Yan, D. Reay, A review on graphene based nanofluids: Preparation, characterization and applications, Journal of Molecular Liquids 279 (2019) 444-484. doi:10.1016/j.molliq.2019.01.153.

[44] A. Asadi, I. M. Alarifi, V. Ali, H. M. Nguyen, An experimental investigation on the effects of ultrasonication time on stability and thermal conductivity of MWCNT-water nanofluid: Finding the optimum ultrasonication time, Ultrasonics Sonochemistry 58 (2019) 104639. doi:10.1016/j.ultsonch.2019.104639.

[45] A. Arshad, M. Jabbal, Y. Yan, Preparation and characteristics evaluation of mono and hybrid nano-enhanced phase change materials (NePCMs) for thermal management of microelectronics, Energy Conversion and Management 205 (2020) 112444. doi: 10.1016/j.enconman.2019.112444.

[46] Dsc 2500, to instruments, uk, accessed: 01/10/2019.
URL https://www.tainstruments.com/dsc-2500/

[47] M. Chieruzzi, A. Miliozzi, T. Crescenzi, L. Torre, J. M. Kenny, A new phase change material based on potassium nitrate with silica and alumina nanoparticles for thermal energy storage, Nanoscale research letters 10 (1) (2015) 273.

[48] R. J. Warzoha, R. M. Weigand, A. S. Fleischer, Temperature-dependent thermal properties of a paraffin phase change material embedded with herringbone style graphite nanofibers, Applied Energy 137 (2015) 716-725.

[49] M. Saterlie, H. Sahin, B. Kavlicoglu, Y. Liu, 0. Graeve, Particle size effects in the thermal conductivity enhancement of copper-based nanofluids, Nanoscale Research Letters 6 (1) (2011) 217. doi:10.1186/1556-276x-6-217.

[50] W. Evans, R. Prasher, J. Fish, P. Meakin, P. Phelan, P. Keblinski, Effect of aggregation and interfacial thermal resistance on thermal conductivity of nanocomposites and colloidal nanofluids, International Journal of Heat and Mass Transfer 51 (5-6) (2008) 1431-1438.

[51] F. Yavari, H. R. Fard, K. Pashayi, M. A. Rafiee, A. Zamiri, Z. Yu, R. Ozisik, T. Borca-Tasciuc, N. Koratkar, Enhanced thermal conductivity in a nanostructured phase change composite due to low concentration graphene additives, The Journal of Physical Chemistry C 115 (17) (2011) 8753-8758. doi :10 .1021/jp200838s.

[52] H. Liu, X. Wang, D. Wu, Fabrication of graphene/Ti02/paraffin composite phase change materials for enhancement of solar energy efficiency in photocatalysis and latent heat storage, ACS Sustainable Chemistry & Engineering 5 (6) (2017) 4906-4915. doi:10.1021/acssuschemeng.7b00321.

[53] H. Tian, W. Wang, J. Ding, X. Wei, M. Song, J. Yang, Thermal conductivities and characteristics of ternary eutectic chloride/expanded graphite thermal energy storage composites, Applied Energy 148 (2015) 87-92. doi :10.1016/j . apenergy .2015.03.020.

[54] J. Wang, H. Xie, Z. Xin, Thermal properties of paraffin based composites containing multi-walled carbon nanotubes, Thermochimica Acta 488 (1-2) (2009) 39-42. doi: 10.1016/j.tca.2009.01.022.

[55] M. He, L. Yang, W. Lin, J. Chen, X. Mao, Z. Ma, Preparation, thermal characterization and examination of phase change materials (PCMs) enhanced by carbon-based nanoparticles for solar thermal energy storage, Journal of Energy Storage 25 (2019) 100874. doi:10.1016/j . est .2019.100874.

[56] M. Mehrali, S. T. Latibari, M. Mehrali, T. M. I. Mahlia, E. Sadeghinezhad, H. S. C. Metselaar, Preparation of nitrogen-doped graphene/palmitic acid shape stabilized composite phase change material with remarkable thermal properties for thermal energy storage, Applied Energy 135 (2014) 339-349. doi : 10.1016/j . apenergy .2014.08.100.

[57] A. A. Aydin, A. Aydin, High-chain fatty acid esters of 1-hexadecanol for low temperature thermal energy storage with phase change materials, Solar Energy Materials and Solar Cells 96 (2012) 93-100. doi : 10.1016/j . solmat .2011.09.013.

[58] E. Hellstern, H. J. Fecht, Z. Fu, W. L. Johnson, Structural and thermodynamic properties of heavily mechanically deformed ru and A1Ru, Journal of Applied Physics 65 (1) (1989) 305-310. doi :10.1063/1.342541.

[59] B.-X. Wang, L.-P. Zhou, X.-F. Peng, Surface and size effects on the specific heat capacity of nanoparticles, International Journal of Thermophysics 27 (1) (2006) 139-151. doi:10.1007/s10765-006-0022-9.

[60] L. Wang, Z. Tan, S. Meng, D. Liang, G. Li, Enhancement of molar heat capacity

of nanostructured a12o3, Journal of Nanoparticle Research 3 (5/6) (2001) 483-487. doi:10.1023/a:1012514216429.

[61] E. V. Timofeeva, J. L. Routbort, D. Singh, Particle shape effects on thermophysical properties of alumina nanofluids, Journal of Applied Physics 106 (1) (2009) 014304. doi:10.1063/1.3155999.

[62] H. Xie, J. Wang, T. Xi, Y. Liu, F. Ai, Q. Wu, Thermal conductivity enhancement of suspensions containing nanosized alumina particles, Journal of Applied Physics 91 (7) (2002) 4568-4572. doi :10.1063/1.1454184.

[63] H. D. Koca, S. Doganay, A. Turgut, I. H. Tavman, R. Saidur, I. M. Mahbubul, Effect of particle size on the viscosity of nanofluids: A review, Renewable and Sustainable Energy Reviews 82 (2018) 1664-1674. do : 10.1016/j .rser . 2017.07.016.

[64] Z. Le-Ping, W. Bu-Xuan, P. Xiao-Feng, X.-Z. Du, Y. Yong-Ping, On the specific heat capacity of cuo nanofluid, Advances in Mechanical Engineering 02 (2010) 1-4. doi: 10.1155/2010/172085.